THE
PHYSICAL REVIEW

A journal of experimental and theoretical physics established by E. L. Nichols in 1893

SECOND SERIES, VOL. 121, NO. 1 JANUARY 1, 1961

Measurement of the g Factor of Free, High-Energy Electrons*

A. A. SCHUPP,† R. W. PIDD,† AND H. R. CRANE
Harrison M. Randall Laboratory of Physics, University of Michigan, Ann Arbor, Michigan
(Received August 17, 1960)

100-kev electrons in 0.1-μsec bunches are sent into a gold foil. The part of the electron bunch which is scattered at right angles, and which, consequently, is partially polarized, is trapped in a magnetic field and held for a measured length of time (up to 300 μsec). The bunch is then released from the trap and allowed to strike a second gold foil. Counters receive the electrons scattered at plus and minus approximately 90°. The cycle is repeated 1000 times per sec. The asymmetry in intensity in the two directions depends upon the final direction of polarization. A plot of the intensity asymmetry vs trapping duration is a cosine curve, whose frequency is the difference between the orbital frequency and the spin precession frequency. This is related to the g factor as follows: $\omega_D m_0 c/Be=a$, where g is $2(1+a)$. Thus the "anomaly," a, is measured directly. The determination of B presents some difficulty because the field must be slightly nonuniform in order to trap the electrons. The spatial variation in B from the center of the trap to the ends is only 0.3%, and the time average of B which applies to the trapped electrons is evaluated to 0.1%. Measurements made at other electron energies, down to 50 kev, showed a slight dependence of a upon energy. The dependence is attributed to electrostatic charges on the surfaces in the trapping region. The final standard error quoted is, however, purposely made large enough so that the variation of a with energy is bracketted. The result is $a=0.0011609\pm0.0000024$.

I. INTRODUCTION

THE research to be described in this report is a continuation of a program which was started many years ago. At that time Louisell, Pidd, and Crane[1] undertook to measure experimentally the gyromagnetic ratio of the free electron by means of a modification of the Mott double-scattering scheme, in which the electrons were made to precess in a magnetic field between the first (polarizing) scatterer and the second (analyzing) scatterer. A result which agreed with the value known from experiments on bound electrons to within the rather wide limits of their experimental error ($\pm\frac{1}{2}$%) was obtained. In the paper in which the experiment was reported,[1] a review of the theoretical and experimental developments relating to the g factor anomaly in bound electrons as well as descriptions of the earlier attempts to measure the g factor of the free electron were given. Therefore, we shall refer to the article mentioned without repeating the discussion of the background material. It will, however, facilitate the description of the present experimental method if we recapitulate the features of the method used by Louisell *et al.*

An electron beam (420 kev) enters a long (30-ft) solenoid in the plane perpendicular to the axis, as shown in Fig. 1, and is scattered by a thin gold foil. The electrons which are scattered through 90° are moving parallel to the magnetic field and are, according to the Mott[2] theory, partially polarized in the direction perpendicular to the direction of motion (axis of the solenoid) and to the direction of the incident beam. At the other end of the solenoid the beam is scattered by a second gold foil into two oppositely place counters, as shown. Again in accordance with the Mott theory, if the beam incident on the second scatterer is polarized there will be an asymmetry in intensity in the two counters and it will be maximum when the line connecting the two counters is normal to the plane of polarization. By plotting the intensity ratio in the counters through 360 deg of rotation of the head, the plane of polarization is determined. The amount of rotation of the plane of polarization which occurs between the scatterers, together with the value of the magnetic field and other constants, gives the g factor. For this purpose the formula of Mendlo-

* This work was supported by the U. S. Atomic Energy Commission.

† Now at General Atomic Corporation, LaJolla, California.

[1] W. H. Louisell, R. W. Pidd, and H. R. Crane, Phys. Rev. **94**, 7 (1954).

[2] N. F. Mott, Proc. Roy. Soc. (London) **A124**, 425 (1929).

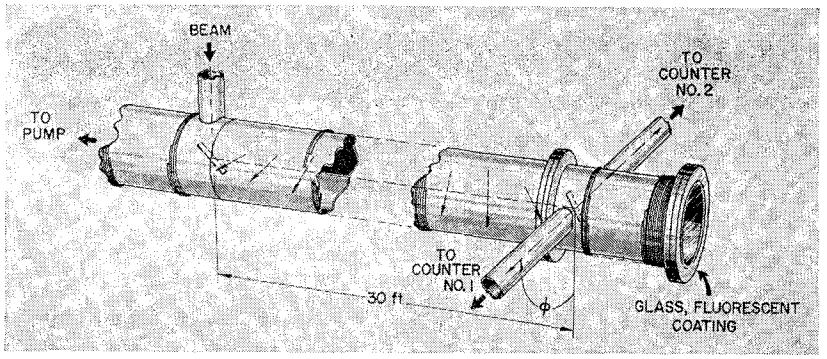

FIG. 1. Schematic diagram of the first apparatus for the measurement of the rotation of the plane of polarization of an electron beam in a magnetic field. The arrows indicate the change in the polarization along the path followed by the electrons.

witz and Case[3] for a beam of Dirac electrons applies. It is, for a beam moving parallel to the magnetic field, $\omega_s=g(eB/2m_0c)(1-\beta^2)^{\frac{1}{2}}$, where ω_s is the angular velocity of the rotation of the plane of polarization.

The experiment just described was limited in accuracy by the small number (5) of cycles of rotation of the plane of polarization that could be observed in the length of path available. Therefore, a modification in the geometrical arrangement was devised,[4] which is the basis of the experiment to be described.

As shown in Fig. 2, the beam, before impinging upon the first scatterer, is parallel to the magnetic field. Electrons which are scattered at about 90 deg follow a helix of small pitch. At the second foil, electrons which are scattered at 90 deg move parallel to the magnetic field, to the right or left. After the first scattering, the direction of polarization is along the radius of the helix, as indicated in the sketch. At the second scattering, radial polarization results in an intensity asymmetry in the two directions parallel to the magnetic field.

If the g factor were exactly 2, the angular velocities of the precession and of the orbital rotation ("cyclotron" rotation) would be identical. In that case the polarization would remain fixed relative to the radius. But since the g factor is expected to differ from 2 by about 0.1% the direction of polarization with respect to the radius is expected to rotate with an angular velocity which is the difference between the angular velocities of the spin precession and orbital motion. The following formulas[3] give the pertinent angular velocities. It should be noted that the spin precession angular velocity for the case in which the velocity is perpendicular to magnetic field (present case) is different from that for the case of the velocity parallel to the magnetic field (as in Fig. 1).

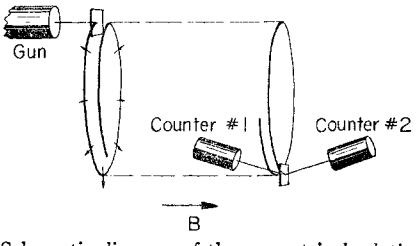

FIG. 2. Schematic diagram of the geometrical relations of gun, scattering foils, counters, and magnetic field, in the present experiment.

$$\omega_c=\omega_0(1-\beta^2)^{\frac{1}{2}},$$

$$\omega_s=\omega_0\left[1+\frac{a}{(1-\beta^2)^{\frac{1}{2}}}\right](1-\beta^2)^{\frac{1}{2}}, \quad v\perp B$$

$$\omega_s=\omega_0(1+a)(1-\beta^2)^{\frac{1}{2}}, \quad v\|B.$$

ω_0 is the "zero energy" cyclotron angular velocity eB/m_0c, and a is the "anomaly" in the g factor, defined by $g=2(1+a)$.

The one further feature of the new experimental scheme is that the magnetic field is modified slightly into a "betatron shape," such as to make it possible to trap some electrons and hold them for an arbitrarily long (and measured) time before letting them strike the second scattering foil. If electrons are so trapped, and if the ratio of the intensities in the two counters is plotted against the duration of trapping, a curve having a sinusoidal modulation of frequency $(\omega_s-\omega_c)/2\pi=\omega_D/2\pi$ sec^{-1} will be expected. The g-factor anomaly, a, is then obtained directly, according to the foregoing formulas, as $a=\omega_D/\omega_0$. Since a is only about 0.001, a measurement of a to a part in a thousand is equivalent to a measurement of the g factor to a part in a million. The only fact that mars this simple relationship is that the trapping process requires the use of a slightly inhomogeneous magnetic field, and since ω_0 is a function of the magnetic field B, it becomes necessary to evaluate the time average of B as experienced by the electrons in the trap. The method of treating this point will be described later.

An important advantage of the new method comes from the fact that injection and counting are separated in time. Consequently no background is caused by the electron gun or the primary beam.

II. APPARATUS

General Layout

A scale drawing of the essential structure of the apparatus is shown in Fig. 3. An aluminum pipe 12 in.

[3] H. Mendlowitz and K. M. Case, Phys. Rev. **97**, 33 (1955); H. Mendlowitz, thesis, University of Michigan (unpublished).

[4] H. R. Crane, R. W. Pidd, and W. H. Louisell, Phys. Rev. **91**, 475 (1953).

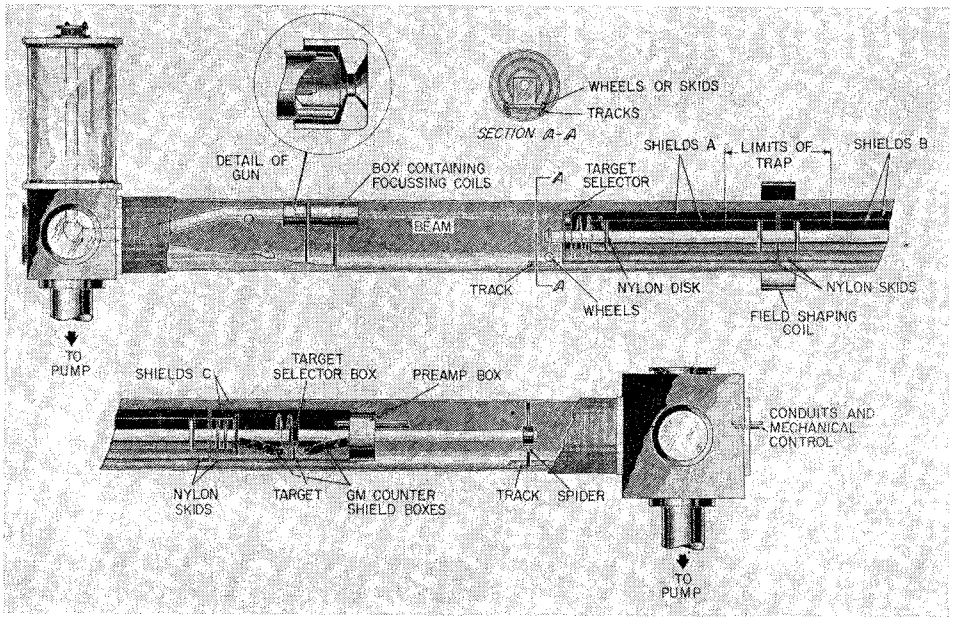

FIG. 3. Drawing of the entire vacuum chamber, including the inner parts.

in diameter and 19 ft long serves as the vacuum chamber and also as the form for the solenoid. At each end there is an aluminum box, in the form of a cube equipped with several manholes and windows. The high-voltage gun is built into one of these boxes. The other box serves little purpose for the g-factor experiment, but it was used for a parallel experiment.[5] A 6-in. oil diffusion pump with refrigerated trap is attached to the bottom of each box. All of the parts which are inside the solenoid can be pulled out in two intact assemblies: One of these is built on a central pipe, 2 in. in diameter and nearly 12 ft long. It can be pulled out through a manhole in the box at the right-hand end, through an appropriately placed hole in the wall of the room, and into the adjoining room. It is provided with wheels and nylon skids, which move along a pair of rails on the inside wall of the solenoid pipe. At the other end a sleeve, 40 in. long, which just fits inside the solenoid pipe is integral with the box. The gun parts are built into this sleeve. The box and sleeve therefore carry the entire gun assembly including the high-voltage accelerating tube. The assembly can be moved out of the solenoid pipe by the aid of a trolly which runs on the ceiling of the room.

High-Voltage Supply

A doubling circuit is used which gives voltages to 120 kilovolts. For regulation a signal is taken from the precision resistor used for the voltmeter. This is converted to ac by an electronic chopper, amplified and rectified. The resulting dc is used in a saturating reactor control in the primary circuit of the high-voltage transformer. This stabilizes the slow variations in the high voltage (0.1 second or longer) to $\pm 1\%$. Rectifier ripple and spikes due to corona discharges are suppressed to within $\pm 2\%$ by the capacitance across the output.

Electron Gun

The electron gun produces a pulsed beam of approximately 100-ma peak current, about 0.1 μsec duration, at a repetition rate of 1 kc/sec. The emitter is a flat spiral of tungsten. This is mounted in a water-cooled cup 1 in. in diameter and $1\frac{1}{4}$ in. deep as shown in the detail of Fig. 3. The cathode assembly is placed inside, and insulated from, the high-voltage electrodes of the gun. The latter is machined from a section of 2-in. diameter aluminum pipe. The electrode is supported on glass legs at one end, and from the top of a 16-in. diameter glass cylinder at the other end. The top of the glass cylinder and the gun are at approximately -100 kv. The assembly can be seen in Fig. 3.

The cathode cup is normally at $+500$ v with respect to the high-voltage electrode, which is sufficient to cut off the electron current. To produce a burst of electrons a negative 3000-v pulse, 0.13 μsec wide, generated by a thyratron pulser is applied to the cathode assembly. The average beam current is measured by placing a collector cup in the path. From this value, and the pulse length and the repetition rate, the instantaneous current is calculated.

Beam Deflection and Focusing Coils

The first scatterer on which the beam must be focussed is about 50 in. in front of the gun. Partial focusing is provided by the main solenoid field, but an additional, controllable, focusing field is needed. This is provided by a small solenoid 10 in. long and 2 in. in diameter. In order to center the beam spot on the polarizer target,

[5] D. F. Nelson and R. W. Pidd, Phys. Rev. **114**, 728 (1959).

horizontal and vertical deflection coils are also provided. These consist of two pairs of rectangular coils $3\frac{1}{2}$ in. wide and 8 in. long. The three sets of coils are located in a vacuum-tight box just in front of the gun shown in Fig. 3, and are supplied with regulated current. When adjusted for typical conditions, the stray field these coils produce in the trapping region, which is 80 in. away, is negligible.

Polarizer Assembly

The targets are mounted on a wheel which is movable from outside the vacuum system. There are four positions: a gold polarizer target which produces the polarized beam, an aluminum target which produces an unpolarized beam necessary for studying possible spurious instrumental asymmetries, a blank target holder used to study background counting rates, and a collector cup used to monitor the beam intensity. The incoming beam is defined by a round hole in a diaphragm ahead of the target position, so that electrons strike only the foil. The position of the polarizer assembly can be seen in Fig. 3.

Solenoid

The selenoid is wound on a form made from two 10-ft pieces of 12-in. i.d., $\frac{3}{8}$-in. wall aluminum pipe, which also serves as the vacuum chamber. The winding consists of four layers of No. 10 B. and S. gauge Formvar-insulated copper wire, close-wound, connected in series. The field at the center is approximately 117 gauss at 6 amperes. Regulation is accomplished by passing the solenoid current through a bank of 48 power triodes (6*AS7*'s) connected in parallel. The triodes are controlled by the output of a high-gain dc difference amplifier whose imput voltages are a reference voltage and a voltage proportional to the solenoid current. The latter is obtained from a diode that is sensitive to magnetic fields (G.E. 2*B*23) placed in an auxiliary coil which is in series with the solenoid. The plate voltage of this diode is used as an input signal for the difference amplifier. The regulator reduces ripple to less than 0.1% and the slow drift to less than 0.05%/hr.

The current in the selenoid is set according to the voltage across a standard shunt as read with a precision potentiometer. The settings are reproducible to less than 0.1%. The magnetic field, in terms of these settings, is found from measurements with a proton resonance device.

Earth's Field Correction Coils

Correction for the earth's magnetic field (as modified by the structural iron of the building) is provided by two rectangular coils, each consisting of 30 turns of wire in wooden forms 28 ft by 5 ft. The long sides of the rectangles and the axis of the solenoid are horizontal, parallel to one another and in the north-south magnetic direction. The planes of the rectangles are horizontal; one is below the solenoid and one above. The coils produce a vertical field in the trapping space of 0.16 gauss/ampere, and the current is set so the vertical component of the earth's field is cancelled. The horizontal component, which is parallel to the solenoid axis, adds to the solenoid field and is taken into account in the calibrations and calculations.

Field-Shaping Coil

The magnetic field is modified slightly so as to produce a region having the "betatron form," by means of an external coil whose field is opposed to that of the solenoid (see Fig. 3). The coil is 18 in. in diameter and 6 in. wide, and contains 593 turns of No. 30 wire in a single layer. The current is regulated by a chopper-type circuit. The field produced by the shaping coil, at the center of the solenoid, is constant to within ± 0.001 gauss.

Internal Potential Shields

The capture of the electrons in the trap and their release is accomplished by applying a pulsed, axial electric field in the trapping region. The trapping procedure will be discussed later; here we shall only point out the structural features. The potential shields consist of three pairs of concentric brass cylinders (*A*, *B*, and *C* in Fig. 3) $9\frac{1}{4}$ in. and $5\frac{3}{4}$ in. in diameter. The electron orbits lie between the larger and the smaller diameter shields. The inner and outer member of each pair are connected together. An axial electric field is produced by applying a potential difference between one pair and another.

Analyzer Assembly

The analyzer assembly consists of a multiple target holder and three Geiger counters. The target holder is controlled from outside the vacuum chamber. A gold foil or an aluminum foil may be lowered into the path of the beam, or the beam may be allowed to pass without striking a foil. Slits before the target restrict the beam to a radial spread of $\frac{1}{4}$ in. The targets are simply curtains of foil which are supported from a point inside the beam radius; consequently, there is no possibility of electrons being scattered by the target holder. Three Geiger counters are used for detecting the scattered beam, two at 80° scattering angles, for the measurement of the asymmetry, and one at 15° as a monitor of the beam intensity. All three are on the "transmission side" of the foil. The counters are standard end-window Geiger counters, $2\frac{1}{2}$ in. long with an inside diameter of $\frac{1}{2}$ in. The central wire, 0.005-in. tungsten, is supported at one end by a glass insulator and is terminated in a bead. The window is 0.00025-in. aluminized Mylar. Each of the counters is enclosed in a lead box $\frac{1}{4}$ in. thick, as a shield against the x rays which are due to the stopping of the electrons which are scattered at other angles.

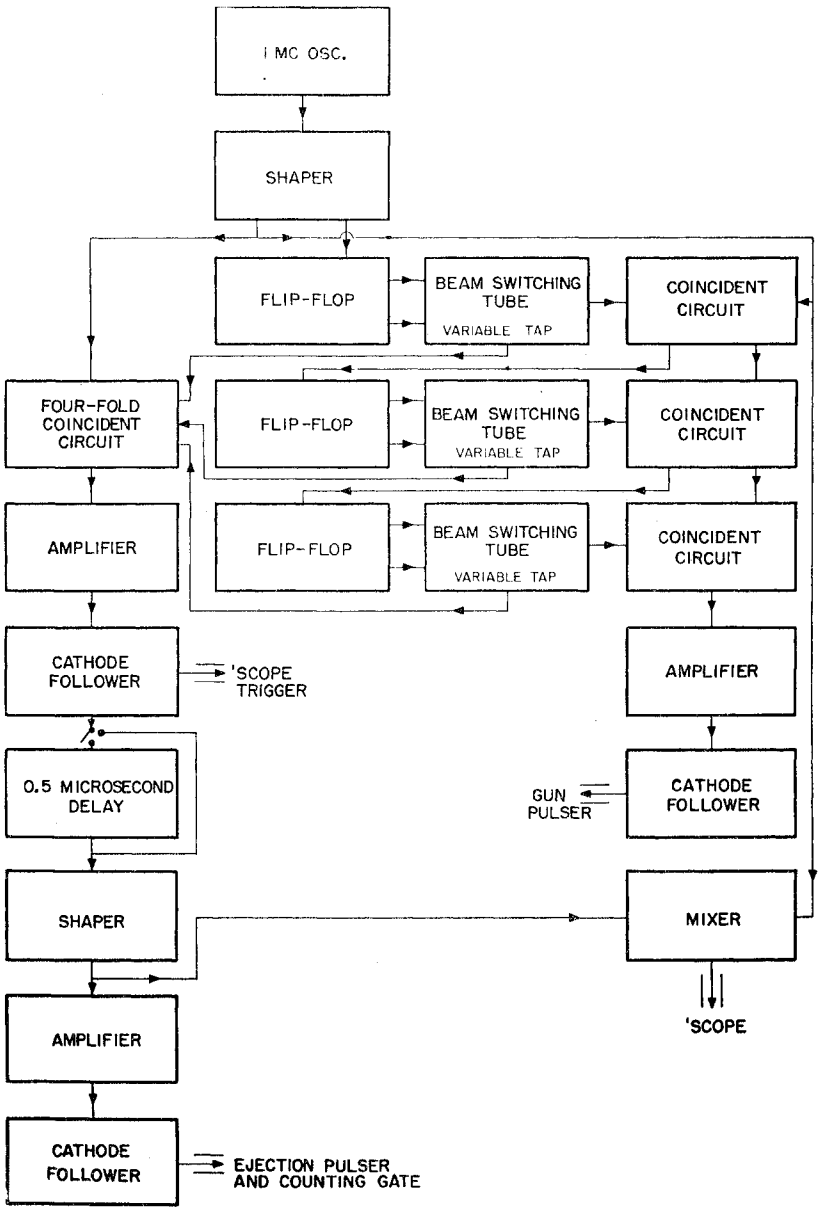

FIG. 4. Block diagram of the master timing circuit.

Control Circuits and Their Operation

Figure 4 is a block diagram of the control circuits. The sequence of events, repeated 1000 times per second, is:

1. A negative potential of 100 v is applied to shield pair B. (A and C are at ground potential.)
2. The gun is pulsed, emitting a 0.13-μsec bunch of electrons.
3. The potential of shield pair B reduced to ground. (This is the change which captures some of the electrons in the trap. It will be called the capture pulse.)
4. The Geiger counters are pulsed up to operating voltage.
5. Shield pair A is pulsed to a negative potential. (This is the ejection pulse.)
6. The counting circuit gates are opened to the scalers.
7. Shield pair A is returned to ground potential.

The only timing circuit that is absolute is the one which controls the interval between capture and ejection. It is shown in block form in Fig. 4. A 1-Mc/sec crystal oscillator with an accuracy of 0.01% is followed by a shaper that generates both positive and negative pulses 0.06 μsec wide and 40 v high. The pulses drive the first of three scale-of-ten circuits, using the Burroughs magnetic beam switching tube No. 6700. This tube has 10 anodes which receive the beam in succession.

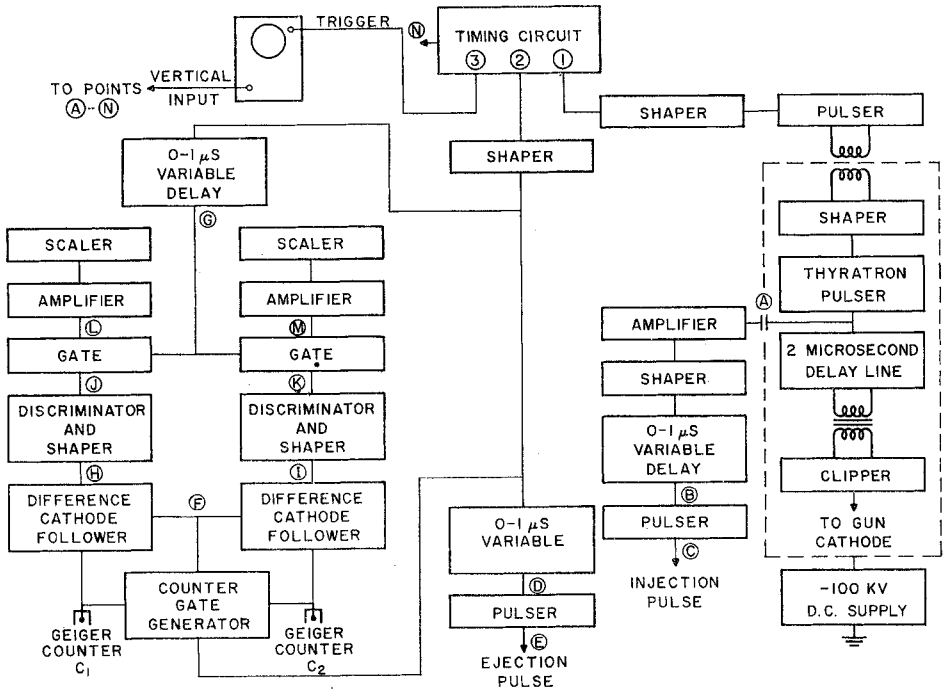

FIG. 5. Block diagram of the electronic equipment.

An output pulse can be obtained from any anode by means of a selector switch. The output from the tenth (zero) anode is fed into a coincidence circuit along with the pulses from the master oscillator so that the output is a pulse in phase with the master oscillator, but delayed by 10 μsec. This pulse drives another scale-of-ten and coincidence circuit, identical to the first, which gives an output pulse in phase with the master oscillator but delayed by 100 μsec. A third stage increases the delay to 1000 μsec. The adjustable output from each scale-of-ten is fed into a fourfold coincidence circuit with the master oscillator pulses, and when there is a coincidence between all four pulses an output pulse is obtained. In this manner, a pulse separated from the pulse of the last anode of the last stage by any interval from 0 to 999 μsec, in 1 μsec steps is obtained. Half-μsec steps are obtained by switching in a fixed $\frac{1}{2}$ μsec delay line ahead of the shaper. A mixer circuit mixes the pulses from the master oscillator with the zero time pulse and the delayed pulse for monitoring with an oscilloscope.

The zero time pulse and the delayed pulse, just discussed, initiate, respectively, the injection and ejection sequences (Fig. 5). The first of these pulses drives a thyratron pulser that transmits a signal to circuits which are at -100 kv. There the pulse is reshaped and used to drive another thyratron pulser that generates a 0.13 μsec, 4000-v pulse for the gun. This pulse is delayed and clipped to 3000 v before reaching the cathode of the gun. Successful trapping depends critically upon the time relationship between the gun pulse and the removal of the negative potential on shield pair B (capture pulse). The capture pulse is therefore triggered by a pulse obtained directly from the gun pulse, through a high-voltage blocking condenser. A 0–1 μsec variable delay line is used for adjusting the capture pulse with respect to the gun pulse. The capture pulse is a 0.5 μsec, 100-v rectangular pulse with a rise time of 0.03 μsec, generated by a delay line pulser.

The second pulse from the timing circuit can be adjusted in time with respect to the first, from 0 to 999.5 μsec. It controls the trapping duration. It turns on the counting circuits and the ejection pulser. A variable delay line is inserted just ahead of the pulser so that the timing of the counting circuits can be varied with respect to ejection.

Counting Circuits

The counting circuit block diagram is shown as part of Fig. 5. The voltage on the Geiger counters is normally at a value below the threshold for counting, and is pulsed into the counting region about 0.2 μsec before the beam is ejected. This time is controlled by the variable delay line just ahead of the ejection pulser. In the injection process a large number of electrons which are not caught in the trap enter the counters. If the counters were continuously at operating voltage, they would discharge at injection and be "dead" for about 100 μsec thereafter. Trapping times of less than the dead time would not be observable. In the scheme used the high-voltage pulse of course appears in the output of the Geiger counter, in addition to the pulse due to the counting discharge. The former is rejected by an anti-coincidence circuit of the cathode follower type which receives the output of the counter as well as a signal from the high-voltage pulser. The Geiger pulse alone is thus obtained, at a low output impedance. These

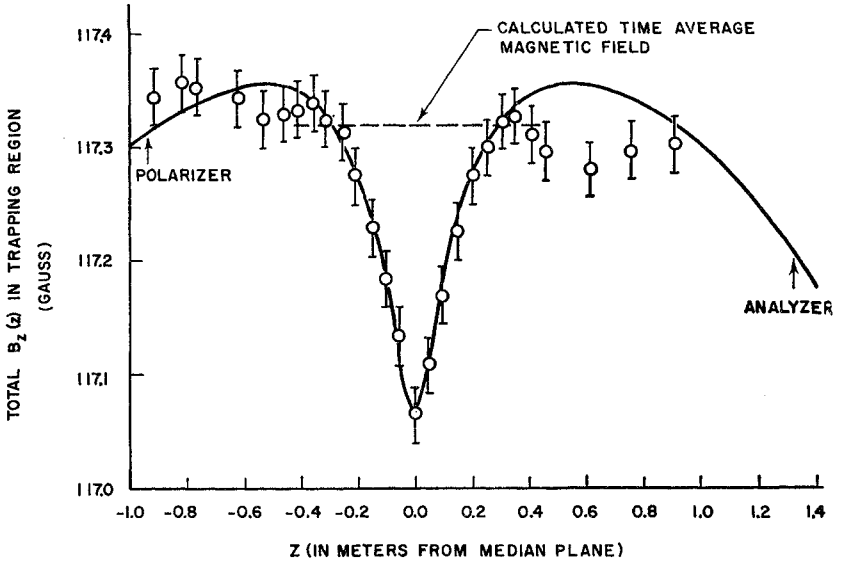

FIG. 6. Total magnetic field. The points are values measured by means of the proton resonance device. The solid curve represents the calculated values.

circuits are situated near the Geiger counters, in a vacuum-tight box within the solenoid. The outputs are fed into a discriminator circuit through a shielded balanced line and then shaped. Another gate circuit is added to insure that only the pulses that occur during a short period of time after the ejection pulse is applied are counted.

III. PROCEDURE OF OPERATION AND CALIBRATION

Trapping

To explain the trapping process, attention is directed to the gap between shield pair A and shield pair B, which is in the plane of symmetry of the trapping region and of the betatron-shaped magnetic field. A 0.13-μsec pulse of electrons enters from the left and strikes the first scatterer. The electrons which are scattered in the favorable direction (only one in 10^5 to 10^6) pursue helical paths of small pitch, progressing to the right and across the gap A-B. At the time the bunch crosses the gap, the difference of potential is 100 v, in such a direction as to reduce the axial momentum of the electrons (or reduce the pitches of the helices). While the bunch is still to the right of the gap, the potential difference is reduced to zero. Therefore when the bunch recrosses the gap, moving toward the left, the lost axial momentum is not regained, and the electrons are permanently caught in the trap, which from that time on is a purely magnetic one. To spill the electrons out at the right-hand end of the trap so that they will proceed to the second scatterer, the process is reversed, applying a potential difference of opposite sign across the gap.

The first success in trapping the electrons was achieved by working with a short trapping time (5 μsec) and a high current in the field shaping coil. After the various adjustments were optimized under these conditions the trapping time was gradually increased and the current in the shaping coil decreased. To maintain trapping when the field was made nearly uniform it was necessary to place, empirically, two small permanent magnets in the neighborhood of the apparatus, one near the gun and one near the trapping region. By careful adjustment of these magnets it was possible to reduce the field of the shaping coil to such a value that the change in axial magnetic field from median plane to the extremities of the trap was only 0.3%, and to hold the electrons in the trap for 600 μsec. Under the final set of conditions used for the experiment, the field contributed in the trapping region by the permanent magnets was less than one part in 10^6 of the main field. The slight gradient they produce is probably the important effect.

Magnetic Field

The magnetic field at the mean radius of the beam (9.53 cm) was computed, in axial and radial components, both for the solenoid and the shaping coil. The field was mapped, experimentally, at the same radius by means of a proton resonance device using a sample consisting of a 0.1M solution of $CuCl_2$ in water. The radio-frequency coil and sample were maintained at the beam radius, but the azimuthal angle and the axial position were varied. The results are shown in Fig. 6. Each point is the average of values obtained over a range of azimuthal angles. The range of variation with azimuth was less than 0.15%. The resonant frequency was found by mixing the oscillator signal from a 500-kc/sec crystal oscillator, and measuring the beat frequency on a calibrated oscilloscope. The earth's magnetic field is cancelled by the correction coils except for

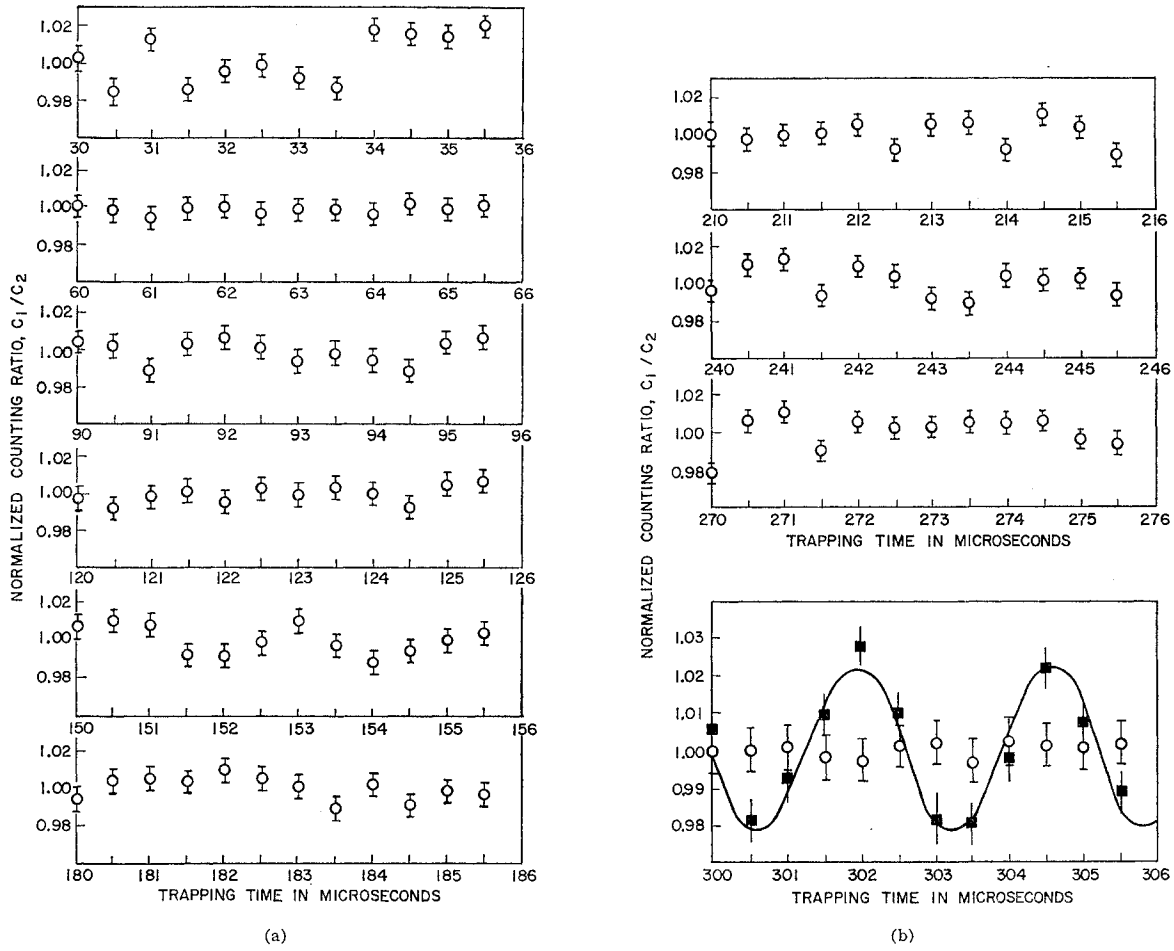

FIG. 7. An experimental test for asymmetry of instrumental origin. An aluminum analyzer was used, in order to reduce the polarization asymmetry to a small value. Circles indicate aluminum analyzer; squares, gold analyzer.

the axial component. This component was measured by reversing the solenoid field, measuring the field at a given point in the solenoid, subtracting this value from the value obtained with the normal field direction, and taking one-half of the difference. It was found to be 0.16 gauss, opposed to the solenoid field.

The values of the two parameters in the calculated field, namely the solenoid and shaping coil currents, which gave the best fit with the experimental points (after correction for the axial component of the earth's field) were then found. They are $I(\text{solenoid})=6.2718$ amperes and $I(\text{shaping coil})=0.01762$ ampere. The currents found in this way agreed with the readings of the current measuring instruments (shunt and potentiometer) to within the limits of accuracy of the latter. After this calibration was once made the solenoid and trapping coils were set according to current, and the field (not including the contribution from the earth) was assumed to be proportional to current, for purposes of shifting to other values of field. The calculated magnetic fields due to the currents in the coils are given in full, in Table I, because the relative contributions are of interest.

Trapping Time Scale

Although the timing circuit generates accurately spaced pulses, the actual time of the first scattering event with respect to the control pulses, has to be determined. By operating the Geiger counters continuously and by keeping the beam intensity low, the pulses which correspond to electrons with large axial momentum, which pass through the trap in negligible time, can be observed on the oscilloscope in relation to the "zero time" pulse from the timing circuit. This measurement shows that 0.6 ± 0.05 μsec is to be subtracted from the times indicates on the timing circuit, to obtain the true trapping time. It may be pointed out that this "end effect" does not enter into the results when the difference frequency is obtained by measuring the number of cycles between two finite ejection times.

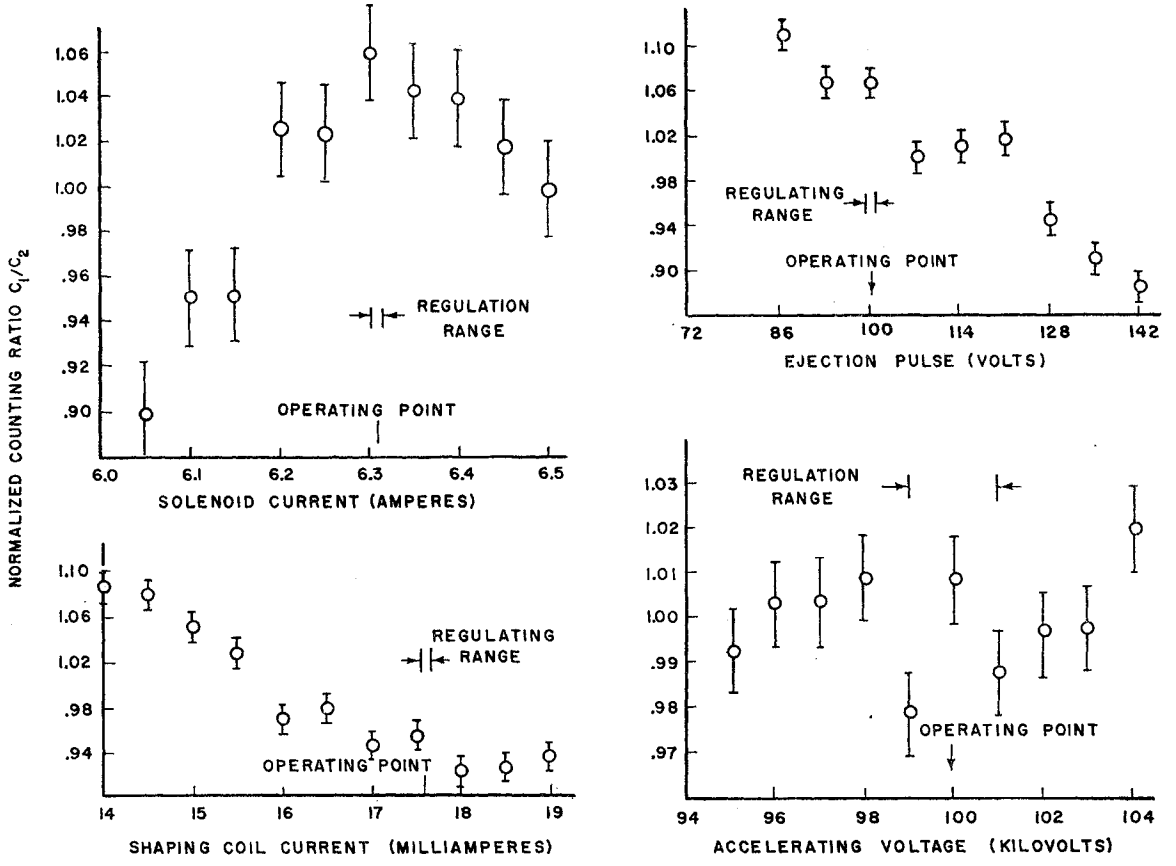

FIG. 8. An experimental test of the sensitivity of the asymmetry to several of the parameters of the apparatus.

TABLE I. Calculated axial and radial components of the magnetic field at the mean beam radius, 9.53 cm.

Z from median plane (meters)	Solenoid $I=6.2718$ amp Axial field (gauss)	Solenoid $I=6.2718$ amp Radial field (gauss)	Shaping coil $I=0.01762$ amp Axial field (gauss)	Shaping coil $I=0.01762$ amp Radial field (gauss)
0.000	117.3900	0.0000000	−0.32000	0.0000000
0.025	...	...	...	0.0170324
0.050	117.3893	−0.0003061	−0.28387	0.0340638
0.075	...	...	...	0.0454194
0.100	117.3886	−0.0006124	−0.22967	0.0526450
0.125	...	...	...	0.0541927
0.150	117.3880	−0.0009185	−0.16516	0.0505800
0.200	117.3874	−0.0012397	−0.12129	0.0387091
0.250	117.3855	−0.0015687	−0.08774	0.0273545
0.300	117.3836	−0.0018979	−0.06193	0.0196127
0.350	117.3808	...	−0.04387	0.0139359
0.400	117.3780	−0.0026041	−0.03200	0.0103221
0.450	117.3746	...	−0.02479	0.0072256
0.500	117.3711	−0.0033784	−0.01909	0.0048510
0.550	117.3665	...	−0.01549	0.0034069
0.600	117.3617	−0.0045584	−0.01238	0.0020640
0.650	117.3570	...	−0.00878	0.0015488
0.700	117.3523	−0.0052324	−0.00722	0.0010325
0.800	117.3385	−0.0063784	−0.00516	0.0005163
0.900	117.3228	−0.0077315	...	...
1.000	117.3027	−0.0093544	...	...
1.100	117.2789	−0.0122691	...	...
1.200	117.2507	−0.0137855	...	...
1.300	117.2174	−0.0168771	...	...
1.400	117.1741	−0.0208455	...	...

Spurious Asymmetries

Spurious asymmetries may be present after second scattering even if there is no Mott asymmetry. A test can easily be made. Since true polarization asymmetry is appreciable only for high atomic number scatterers, an aluminum analyzer target is a convenient tool with which to isolate such spurious asymmetries.

One class of spurious asymmetries is related to the geometry of the system: asymmetric scattering angles to the counters, asymmetry in the magnetic field, and misalignment in the slits, counters and target holders. The scattering angle for one of the counters is not quite the same as that for the other due to the fact that the beam travels in a helix and, therefore, strikes the analyzer target at a slight angle. The two counting rates are, therefore, different due to the dependence of the scattering cross section on angle. The angle of incidence may not be independent of trapping time for very short trapping time, since it depends on the axial momentum given the beam on ejection which, in turn, depends on the position of the electron bunch at the instant of ejection. Results for the aluminum analyzer are shown in Fig. 7. For comparison, results obtained under the same conditions with a gold analyzer are shown for the 300 to 305.5 μsec interval. The error flags shown are

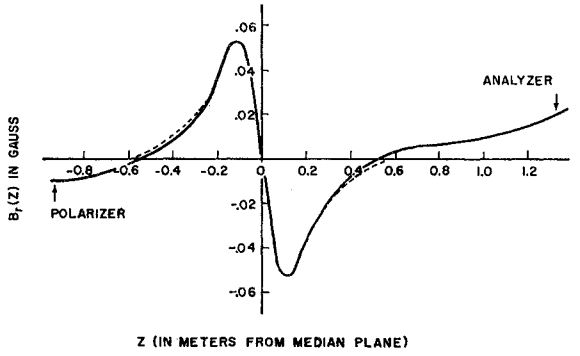

FIG. 9. Plot of the total radial magnetic field at the orbit radius, according to the calculated values in Table I.

those due to statistical fluctuations in the number of counts. The conclusion drawn from these tests is that no correction for asymmetries of geometrical origin is necessary.

Another class of asymmetries is related to the adjustment of the electrical parameters of the system: the currents in the solenoid and shaping coil, and the height of the pulse used for ejection and the kinetic energy of the electron beam. Since these parameters are constant only within limits, during a run, it is desirable to know how critically they affect the asymmetry. To this end, runs were made using the aluminum analyzer, in which the parameters mentioned were varied individually. The results are shown in Fig. 8. From these graphs it can be seen that spurious asymmetries of this type are small ($<0.5\%$) and are negligible compared to the Mott asymmetry. Drifts of this type are slow compared to the time necessary to measure the difference frequency in one of the 5.5-μsec sections, so it can cause only a gradual shift of the counting ratio, with negligible effect on the difference frequency.

Determination of the Time-Average Axial Magnetic Field

As mentioned earlier, it is necessary to estimate as accurately as possible the time average of the axial component of magnetic field which the electron experiences while in the trap, in order to compute the value of the g factor from the difference frequency. The error associated with this estimate is minimized by using a field which is as nearly uniform as is possible, consistent with holding the electrons in the trap. For all of the measurements of difference frequencies, the maximum variation in the axial field, from the ends of the trap to the center, was only about 0.3%, as is seen in Fig. 6. Thus the entire range corresponds to only about 3 parts per million in the g factor. However, we wish to attempt a closer estimate. To do so we must describe some of the detailed properties of the trap.

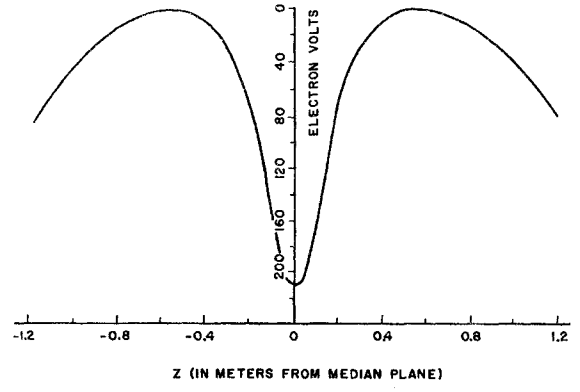

FIG. 10. Effective potential well for 100-kev electrons.

The total radial component of magnetic field at the orbit radius, taken from Table I, is shown by the solid line in Fig. 9. This applies to the solenoid and shaping coil settings used in the experiments at the highest energy, 100 kev. When lower energy electrons were used, only the current in the solenoid was reduced; the current in the shaping coil was the same at all times. The total radial field does not vary appreciably, because the contribution from the solenoid is small. The dotted line in Fig. 9 shows the total radial field in the case of the lowest energy, 50 kev.

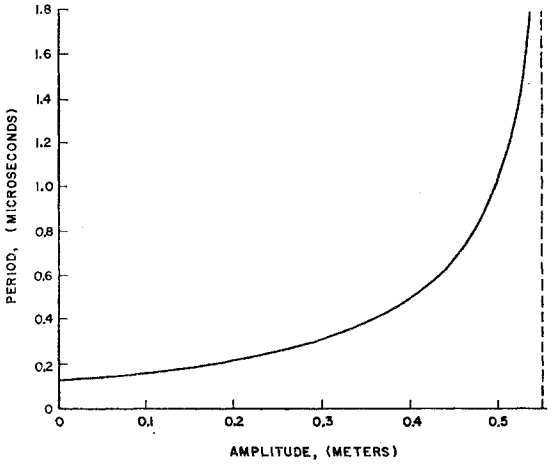

FIG. 11. Period of oscillation vs z amplitude, for a 100-kev electron in the trap.

The total velocity of a trapped electron is constant, as it moves in a static magnetic field. The maximum pitch of the helical motion in the trap is about 3 degrees, a value which comes out of the calculation at a later point. Consequently, the azimuthal component of velocity, V_ϕ, varies by less than 0.3%, and it can be considered to be constant for our immediate purpose. The axial force, $F_z=(eV_\phi/c)B_r(z)$, can therefore be considered to be a function of only one variable, namely z. We have what amounts to a potential well for the electrons, and we may plot it in terms of electron volts. It is shown in Fig. 10. The period as a function of amplitude can be found by graphical integration. It is shown in Fig. 11.

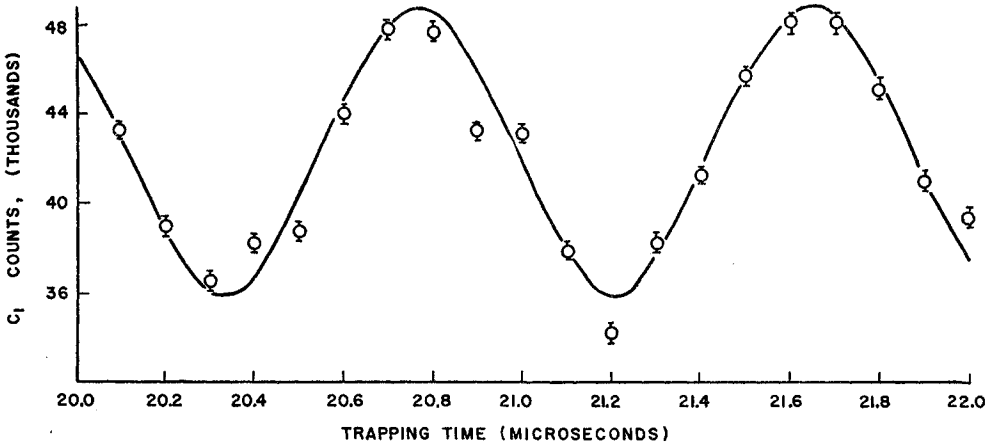

FIG. 12. Number of electrons ejected from the trap vs trapping time for short times.

The period of z oscillation in the trap was measured experimentally. At the instant the electrons are trapped, they are all on one side of the median plane. They remain bunched for the first few periods of axial (z) oscillation. If the ejection pulse is applied within this short time, the number of electrons which leave the trap will be time dependent. The electrons leave the trap and go to the counters (to the right) only if the bunch is on the left side of the median plane at the time the pulse is applied. The result of such a measurement for electron energy 100 kev is shown in Fig. 12. The period is 0.88 μsec.

The period observed fixes the amplitude at 0.487 meter, indicating that most of the trapped electrons have z amplitudes which are about 90% of the length of the trap. At that amplitude the curve of amplitude vs period is quite steep. Therefore, since the electrons remain bunched for such a long time, we conclude that they occupy only a very narrow energy band in the potential well. The spread in period must not be more than a few percent, and this implies (referring to the curves of Figs. 10 and 11) that the spread in energy in the well must not be more than a few ev.

The above result is surprising, in view of the fact that the trapping procedure, in principle, admits an energy band whose width is as great as the change in potential applied to the shields at the instant of capture, namely about 100 ev. We therefore postulate that imperfections in the magnetic field impose a further restriction on the energy band (or z amplitude) which can exist in the trap. We know, from the way in which the final adjustments are made, that imperfections are important. The trap, for reasons already explained, is extremely weak (0.3% maximum variation in field). After trapping is initially accomplished in a stronger trap, the gradual reduction to the 0.3% variation is possible only if small, empirical adjustments, including the placing of two small permanent magnets in the neighborhood of the solenoid are made.

An important imperfection which is to be expected in a weak trap is a lack of coincidence between the magnetic axis and the physical axis of the apparatus. We believe this can account for the observed restriction on the permitted z amplitude, in the following way. If the axis of the helix into which the electrons are launched at injection does not coincide with the magnetic axis, the former will drift around the latter, at constant distance from it. If there is appreciable separation (2 cm or more) between these two axes, there will not be room enough for the drift motion, and the electrons will strike the walls. The angular velocity with which the one axis drifts around the other is given by

$$\omega_r-\omega_c=\omega_c[(1-n)^{\frac{1}{2}}-1]\simeq-\tfrac{1}{2}\omega_c n \simeq-\tfrac{1}{2}\omega_c\frac{r}{B_z}\frac{\partial B_r}{\partial z},$$

where $n=(r/B_z)(\partial B_z/\partial r)=(r/B_z)(\partial B_r/\partial z)$ and ω_c is the "cyclotron" angular velocity. The sense of the drift reverses where $\partial B_r/\partial z$ changes sign, that is, at each of the crests of the curve in Fig. 9. There will be a value of the z amplitude (greater than the distance between the two crests) for which the time average of $\omega_r-\omega_c$ is zero. (Such a solution must exist, since the time spent beyond the crests can take any value from 0 to ∞, according to Fig. 11.) For electrons which satisfy this condition as to z amplitude, the axis of the helix will merely oscillate back and forth over a small range rather than drift all the way around the physical axis. In this way the drift which normally causes the beam to destroy itself by striking the wall does not occur.

The foregoing mechanism is subject to the condition that the drift of the one axis around the other is slow compared to the z oscillation in the trap. A check is made as follows: the falloff index, n has its maximum value at the center of the trap, and is (for the 100-kev setting) 0.0006. This gives a maximum for $\omega_r-\omega_c$ of 0.4×10^6 rad/sec, which is the rate of 0.1 radian per quarter-period of the z oscillation. This places an upper limit of ±0.1 radian for the excursions of the axis. The criterion is well satisfied.

TABLE II. Results of the computation of the time-average magnetic field for trapped electrons of the eight different energies used in the experiments.

Electron energy kev	Shunt reading (volts)	Time average magnetic field (gauss)	Electron energy kev	Shunt reading (volts)	Time average magnetic field (gauss)
50	0.5819	82.074	81	0.7500	105.830
58	0.6286	88.674	95	0.8000	113.056
60	0.6500	91.698	98	0.8212	115.892
70	0.7000	98.764	100	0.8313	117.319

The ratio of the number of final counts to the number of electrons incident on the first foil, per pulse, is consistent with the assumption that only a very small energy interval in the potential well is occupied. The cross section for scattering by a gold nucleus at 90 deg and 100 kev ($\beta=0.55$) is about 6×10^{-21} cm^2/steradian.[6] A 3-ev interval in the potential well corresponds to a 10^{-4} radian interval in the angle of first scattering, in the plane parallel to the solenoid axis. The interval in angle in the plane normal to the solenoid axis which will be accepted can be estimated from the spacing between the internal shields. It is taken to be 0.1 radian. Thus the solid angle accepted after the first scattering is 10^{-5} steradian. The solid angle subtended by the counter at the second scatterer is $\sim$0.03 steradian. The number of electrons incident on the first scatterer is about 8×10^{10} per pulse. The foregoing figures combine to give an expected count of 0.3 per pulse. This is to be compared with the observed counting rate, which ranged from 0.1 to 0.01 count per pulse, depending on the trapping duration.

The consistency of the data with the foregoing analysis leads us to adopt the value of 0.487 meter for the z amplitude for all of the electrons in the trap. The same amplitude is taken to apply to the experiments at the several values of electron energy, because (a) the radial magnetic field is very nearly independent of B_z (Fig. 9), and (b) the z amplitude which satisfies the condition $\omega_r-\omega_c=0$ is independent of B_z in first order (the z motion depends on B_r, and B_z is only a multiplicative constant for $\omega_r-\omega_c$). In computing the values of time-average axial field it was assumed that the contribution of the main solenoid is proportional to the current and that the axial contributions of the shaping coil and the earth were constant. The values are listed in Table II.

IV. RESULTS AND ANALYSIS

Measurement of the Difference Frequency

The trapping time was varied in steps of 0.5 μsec over the range of 30 to 305.5 μsec, and the counting rate ratio was measured at each setting. 25 groups of 12 points, each group extending over 5.5 μsec, were taken. The set which will now be described in detail is the main one and it consists of 13 groups of 12 points taken at 100-kev electron energy. The runs in this set cover the first 5.5 μsec of each 30-μsec interval, from 30 to 300 μsec, with the last run repeated four times. The data are shown in Fig. 13.

The first step in the analysis is to determine the number of cycles between 0 and the last maximum, in order to obtain a value for the period, which will be used in the second step. This is done by fitting, visually, a cosine curve to the points, with particular attention to the interval at the top end (300–305.5 μsec) since there are four runs in that interval. We estimate that this fit can be made to within $\frac{1}{8}$ period, at the top end. The estimate of the period will therefore be accurate to about one part in 1200, provided the number of cycles assumed to lie between the origin and the top interval is not in error by a whole number. The possibility of such an error is tested by attempting to fit cosine curves having one more, and one less, cycle than the number assumed to be correct. When this is done the disagreement in the middle part of the series seems to us to be decisive. In Fig. 13 small arrows are inserted to indicate the positions of the crests of the cosine curve which was used. Arrows with + and − signs indicate, respectively, the crests of cosine curves in which one more, or one less, cycle is introduced, respectively.

The second step is as follows: A cosine curve having the period just found is adjusted to each 5.5-μsec group of points, independently. The amplitude of the cosine curve is varied, and it is slipped along the abscissa until a least squares solution is found. The operation is carried out using an IBM 650 computer. The time in μsec from the origin to the first maximum in the cosine curve which falls within the 5.5-μsec interval is found in each case. The results (M_i) are given in the first column of Table III. Since less than two cycles of the cosine curve fall within the 5.5-μsec interval, the result for M_i is not sensitive to the value of the period used in the fitting process. The preliminary estimate

TABLE III. Results of fitting a cosine curve to each 5.5-μsec section of the counting ratio vs trapping time data. M_i is the trapping time corresponding to the maximum of the cosine curve.

Run No.	Energy (kev)	M_i (μsec)	Run No.	Energy (kev)	M_i (μsec)
I	100	32.030	XIV	98	300.346
II	100	60.822	XV	81	302.657
III	100	92.307	XVI	70	203.042
IV	100	121.128	XVII	70	252.321
V	100	152.507	XVIII	70	268.062
VI	100	181.164	XIX	70	281.120
VII	100	210.189	XX	70	302.003
VIII	100	241.346	XXI	60	252.236
IX	100	270.422	XXII	60	301.776
X	100	301.703	XXIII	60	301.745
XI	100	301.941	XXIV	58	301.990
XII	100	301.913	XXV	50	303.266
XIII	100	301.961			

[6] Noah Sherman, Phys. Rev. **103**, 1601 (1956).

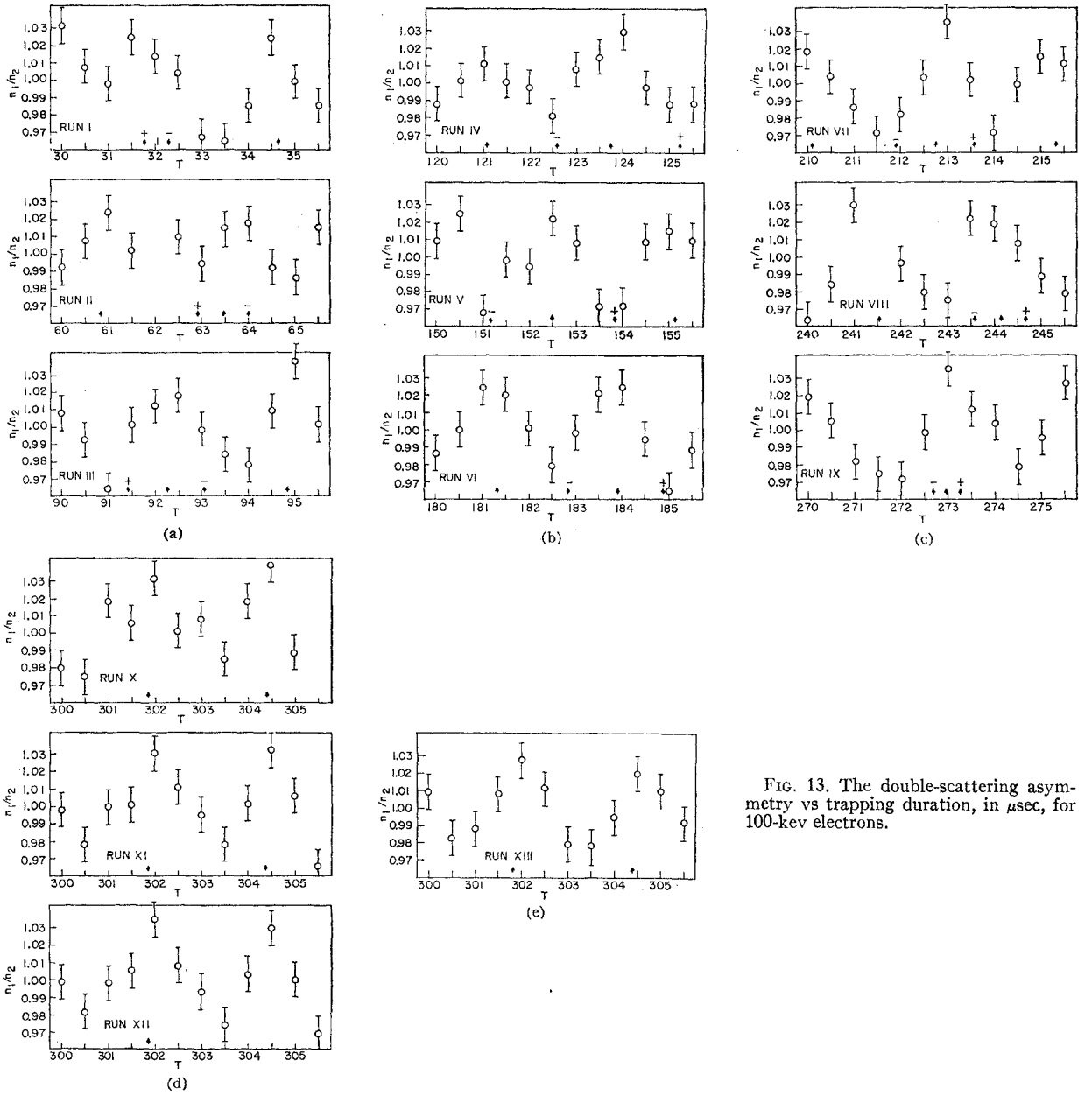

FIG. 13. The double-scattering asymmetry vs trapping duration, in μsec, for 100-kev electrons.

of the period made in step one is of more than sufficient accuracy for the purposes of step two.

In addition to the main series, I to XIII, similar runs over 5.5-μsec intervals were made at different values of electron energy and magnetic field. These were analyzed in the way just described, except that in some electron-energy groups there were not enough runs to permit an independent determination of the total number of cycles. The information was obtained readily by reference to the main series (I–XIII) and by intercomparisons. The runs (XIV–XXV) are shown in Fig. 14, and the values of M_i are given in the right column of Table III.

Finally, two sets of runs were taken which check particular estimates used in the evaluation of the final result. The first of these is a single, continuous run, at 95 kev, from 30 to 130 sec (Fig. 15). A cosine curve was fitted to this run by the least squares method. When this was extended to the left, the zeroth maximum was found to be displaced 0.6 ± 0.1 μsec to the right of the zero of the abscissa scale, in confirmation of the direct measurement of the zero time correction described earlier. The second of these sets comprises 15 runs over the 300–305.5 μsec interval at 100 kev, with identical settings of the parameters but scattered in time over an interval of three weeks. The object was to obtain an experimental value for the rms deviation of M_i from the mean. It was found to be 0.3 μsec.

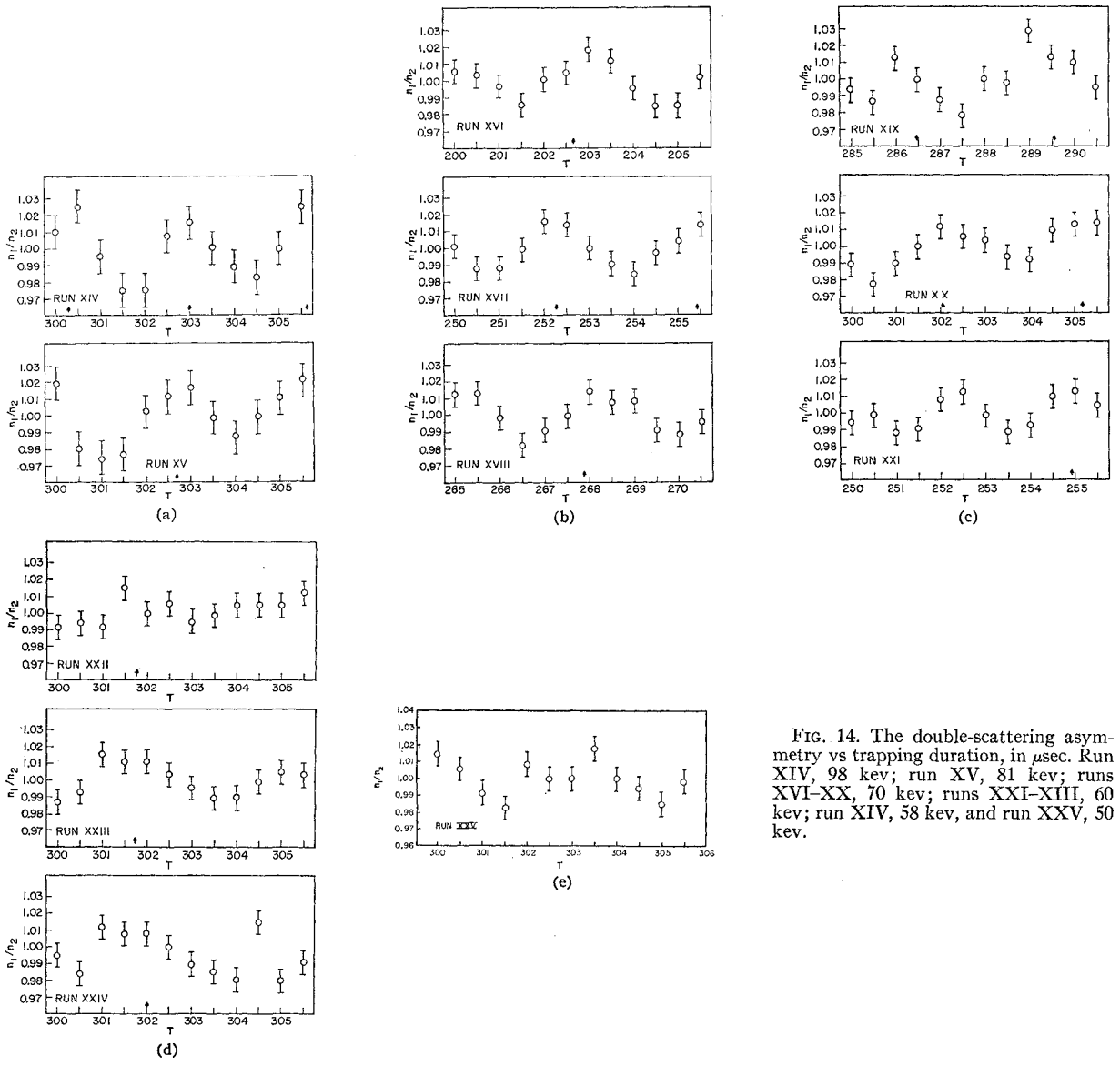

FIG. 14. The double-scattering asymmetry vs trapping duration, in μsec. Run XIV, 98 kev; run XV, 81 kev; runs XVI–XX, 70 kev; runs XXI–XIII, 60 kev; run XIV, 58 kev, and run XXV, 50 kev.

Computation of the Anomaly

We wish to use the M_i values in Table III to obtain a properly weighted average value of $a=\omega_D/\omega_0$, for each group having a particular electron energy.

$$a_i=2\pi N_i mc/(M_i-t_0)B_i e,$$

where N_i is the number of cycles measured from the origin, t_0 is the "end effect" correction to the time scale and B is the magnetic field. For purposes of making the weighted average of a, we consider only the nonsystematic errors in M_i, t_0, and B_i, i.e., those which are associated with the number of counts, with the resetting of the meters and timing circuits from one day to another, with temperature and power line fluctuations, etc. We postpone the introduction of the estimated systematic errors to the stage at which we will have a single value of a.

The standard error in the least-squares fit of the cosine curve to the points in the 5.5-μsec interval is difficult to determine analytically. We estimate it to be 0.3 μsec. The experimental rms deviation in M_i (described earlier) which may include fluctuations of origin other than the statistical ones is no larger than the 0.3 μsec here adopted; therefore we believe that the estimate is conservative. We estimate the standard error of nonsystematic origin in B to be 0.05% and that in t_0 to be 0.05 μsec. The error in M_i is the most important, since it ranges from 0.1% at 300 μsec to 1% at 30 μsec. When the above three errors are combined for each a_i and when all a_i for a given electron energy are combined in a weighted average, the values in Table IV are found.

Systematic errors are estimated, and given in terms

of standard (0.7 probability) errors. They may be listed under three headings.

1. Systematic errors which are of the order 0.01% or smaller, and which therefore affect the final result for a by 0.1 part per 10^6 or less. These are: (a) The absolute time rate. This was checked against *WWV*. (b) The proton resonance mapping of the magnetic field. (c) The values of the physical constants, including the proton g factor. (d) The measurement of the high voltage. While this measurement is only good to 1%, it does not enter the final result in first order. Its effect on ω_D/ω_0 comes only through its effect on the radius of the orbit and through interaction with stray radial electric fields in the trapping region. (e) Axial electric field. The axial restoring force, toward the median plane, is due mainly to B_r, but it can also contain a small contribution from an axial electric field, if one is present. The latter would be present only as the result of contact potential differences or surface charges. The change of potential across the trapping region, due to these causes, would not be expected to be more than the order of 0.1 volt. Since the effective potential well due to B_r is about 200 volts deep, axial electric field effects are considered to be negligible. (f) The effect of B_r on the precession. If the electron remains in the trap, the time average of the z force must be zero; therefore, assuming that the force is due entirely to B_r, the time average of B_r at the electron must be zero. The z oscillation frequency is higher than the "difference frequency" so we expect the precession of the spin axis caused by B_r to average to zero. (g) The pitch of the helix. The time average of the absolute value of the pitch angle, α, can be computed from the known z amplitude and z frequency. It is about 0.7 deg. The effect of pitch angle upon ω_D has been calculated. All terms are antisymmetric in α, and therefore have a time average of zero except one, which is

$$\left(\frac{1-(1-\beta^2)^{\frac{1}{2}}}{(1-\beta^2)^{\frac{1}{2}}}\right)\sin^2\alpha,$$

compared to 1. An estimate of the time integral of the above term over a cycle of the z motion indicates that the pitch angle effect is of the order of 0.01% and therefore negligible.

2. Systematic error in the determination of the time average magnetic field. This is a complicated procedure (already described). The standard error assigned (0.1%) seems to be generous, since it is about $\frac{1}{3}$ the entire range of B in the trapping region. It enters linearly, so it amounts to 1 part per 10^6 in the final result for a.

3. Stray radial electric fields in the trapping region. This is a possible source of systematic error whose importance can be inferred only from an analysis of the data. Such fields could be caused by the charging of insulating specks on the surfaces by the electrons and by contact potentials. The effect would be to add a term to the equation for ω_D/ω_0 as follows:

$$\frac{\omega_D}{\omega_0}=a+\frac{\bar{E}_r}{cB}\left(\frac{\beta^2-1}{\beta}+a\beta\right).$$

A radial E of approximately 20 volts/cm (time-averaged over the path of the electron) would reduce ω_D to zero. Since, in the above expression the orbit radius, r, is constant, B and β are related. Therefore β can be eliminated, as follows:

$$\frac{\omega_D}{\omega_0}=a+\frac{\bar{E}_r(aB^2K^2-1)}{cB^2K(1+B^2K^2)^{\frac{1}{2}}},$$

where $K=re/m_0c^2$.

In the range studied, K^2B^2 varies from 0.21 to 0.44, and $aB^2K^2\ll 1$. Therefore, on a $1/B^2$ scale, in the range

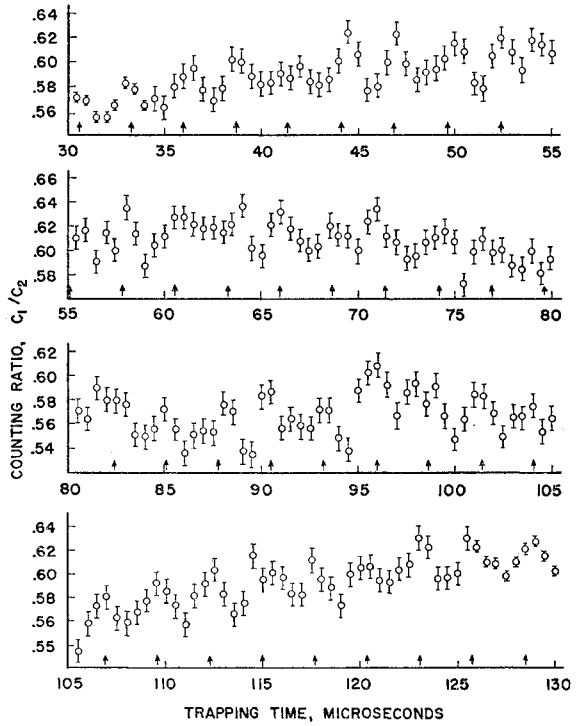

FIG. 15. The double-scattering asymmetry vs trapping duration in a continuous run from 30–130 μsec.

TABLE IV. The g-factor anomaly a, or ω_D/ω_0 calculated for the various electron energies, prior to the introduction of the estimated systematic errors.

B (gauss)	Energy (kev)	ω_D/ω_0	Standard error
82.074	50	1.16448×10^{-3}	1.24×10^{-6}
88.674	58	1.16255×10^{-3}	1.23×10^{-6}
91.698	60	1.16308×10^{-3}	0.74×10^{-6}
98.764	70	1.16346×10^{-3}	0.62×10^{-6}
105.830	81	1.16224×10^{-3}	1.21×10^{-6}
115.892	98	1.16168×10^{-3}	1.20×10^{-6}
117.319	100	1.16232×10^{-3}	0.45×10^{-6}

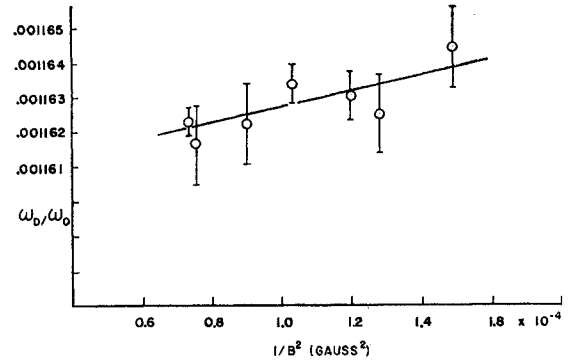

FIG. 16. Plot of ω_D/ω_0 vs $1/B^2$.

considered, ω_D/ω_0 is nearly a straight line whose slope is proportional to $\bar{E}_r$. The values of ω_D/ω_0 from Table IV plotted against $1/B^2$ are shown in Fig. 16. A least squares fit of a straight line to the points gives a slope which indicates that $\bar{E}_r=0.04$ v/cm with an estimated uncertainty of 0.02 v/cm. When this value of $\bar{E}_r$ is inserted in the equation (which itself represents nearly a straight line) the value of a which produces tangency with the least square straight line at the middle of the $1/B^2$ range is 0.0011609.

The foregoing analysis must be treated as being based upon an uncertain hypothesis. While a stray radial electric field of some small value certainly is present, it is by no means certain that it accounts fully, or even mainly, for the slope in the $1/B^2$ plot. Two weaknesses in the hypothesis that the slope is due to an electric field are: (a) The behavior would be expected to be erratic due for example to changes in the condition of the metal surfaces. Positive indication of this was searched for but not found. The trend was not found to be correlated with the age of the apparatus. The runs at different voltages were not made in order, but were purposely "scrambled," yet they fell into place on the sloping line. On several occasions in the course of the experiment the apparatus was opened and the surfaces were cleaned. This would be expected to change the tendency of the surfaces to hold charges, but no abrupt change was observed. (b) The assumption that the electric field is the same for all the values of electron energy is open to objection. Although the orbit radius is the same for different voltages, a dependence of the number of electrons lost to the surfaces on energy would not be unexpected. Thus the possibility that the trend of the value of a with electron energy is due to some other instrumental cause, or even that there is a real dependence not included in present theory cannot be excluded.

In deciding upon a single value for a to give as the result of the experiment, our judgement is that we should recognize the trend of the points in Fig. 16, and proceed on the assumption that a radial electric field is present, in spite of certain weaknesses in the evidence for it. The value $a=0.0011609$, obtained in this way, may be compared with a simple weighted average of the data of Table IV, which is 0.0011627. We adopt the value 0.0011609 but assign a standard error which is great enough to include the weighted average of Table IV, namely ± 0.0000020. Finally, we combine with this the estimated systematic standard errors. The principal one of these is the one concerned with the estimate of the time average magnetic field (1 part per 10^6 in a). The others are considerably smaller. We use 1.4 parts per 10^6 for the group. This results in a final value of $a=0.0011609\pm 0.0000024$.

V. COMPARISON OF RESULTS WITH CALCULATIONS AND WITH OTHER EXPERIMENTAL RESULTS

In 1948 Schwinger[7,8] expressed the g factor as a series of radiative correction terms added to the Dirac value of 2, in powers of the fine structure constant. The term in first order in α was calculated by Schwinger with the result:

$$g_e=2(1+\alpha/2\pi)=2\times 1.00116138.$$

The second-order term in α was evaluated by Karplus and Kroll[9] and by Sommerfield.[10] The results were

$$g_e=2(1+\alpha/2\pi-2.973\alpha^2/\pi^2)=2\times 1.0011454,$$

(Karplus-Kroll)

$$g_e=2(1+\alpha/2\pi-0.328\alpha^2/\pi^2)=2\times 1.0011596.$$

(Sommerfield)

Recently this difference has been resolved and the accepted value is 2×1.0011596. It is in agreement with the bounds calculated by Petermann.[11]

A number of experiments have been reported that determine the magnetic moment and g factor of an electron when bound in an atom. Kusch and Foley[12] have shown that $g_e=2(1.00119\pm 0.00005)$ by atomic beam measurements of the Zeeman effect in the ground state of Ga, In, and Na. A more precise determination is achieved by combining the results of two separate experiments. One type of experiment determines the magnetic moment of the proton in units of the Bohr magnetron, (μ_p/μ_0) and the other determines the ratio of the magnetic moment of the electron to the magnetic moment of the proton (μ_e/μ_p). The product of these two results gives the magnetic moment in Bohr magnetons or one-half the g factor for the bound electron. By applying suitable relativistic corrections the magnetic moment of the free electron can be obtained.

In 1949 Taub and Kusch[13] made the first determination of μ_e/μ_p by a molecular beam magnetic resonance

[7] J. Schwinger, Phys. Rev. **73**, 416 (1948).
[8] J. Schwinger, Phys. Rev. **74**, 1439 (1948); **75**, 651 (1949); **76**, 790 (1949).
[9] R. Karplus and H. M. Kroll, Phys. Rev. **77**, 536 (1950).
[10] C. M. Sommerfield, Phys. Rev. **107**, 328 (1957).
[11] A. Petermann, Nuclear Phys. **5**, 677 (1958).
[12] P. Kusch and H. M. Foley, Phys. Rev. **74**, 250 (1948).
[13] H. Taub and P. Kusch, Phys. Rev. **75**, 1481 (1949).

method. They measured the frequency corresponding to a reorientation of the proton in the molecule NaOH and the frequency corresponding to a transition between certain of the hyperfine structure levels of the ground state of both Cs^{133} and In^{115}. By combining this result with measurements obtained in related experiments,[14,15] they found that

$$\mu_e/\mu_p(\text{NaOH})=658.21\pm0.03.$$

The most precise values of μ_e/μ_p for a bound state are obtained by observing the ratio of the electronic-spin g value of atomic hydrogen in the $^2S_{\frac{1}{2}}$ state to the proton g value in a sample of mineral oil or water, in the same magnetic field. A relativistic correction is applied to account for the binding energy of the electron in the hydrogen atom and then μ_e/μ_p for the free electron is obtained. Three results have been published by different groups[16–18] using the above methods and the results are all in agreement to within 2 parts per million. The average of their results yield $\mu_e/\mu_p(\text{oil})=658.2292\pm0.0012$. A least-squares analysis made by DuMond and Cohen in 1955, recently reviewed by DuMond[19] gave 658.2288 ± 0.0004.

A determination of $\mu_p(\text{oil})/\mu_0$ has been completed by Gardner and Purcell[20] and independently by Franken and Liebes.[21] In these experiments the ratio of the nuclear magnetic resonance frequency of protons to the cyclotron frequency of free low-energy electrons was determined. Both frequency determinations were performed as nearly as possible in the same location in the magnetic field so that a measurement of the magnetic field was not necessary. The results of these experiments were

$$\mu_0/\mu_p(\text{oil})=657.475\pm0.008 \text{ (Gardner-Purcell)},$$
$$\mu_0/\mu_p(\text{oil})=657.462\pm0.003 \text{ (Franken-Liebes)}.$$

When these results are combined with the value for $\mu_e/\mu_p(\text{oil})$ the following values for the g factor are obtained:

$$g_e=2(1.001146\pm0.000012) \text{ (Gardner-Purcell)},$$
$$g_e=2(1.001165\pm0.000005) \text{ (Franken-Liebes)}.$$

The Gardner and Purcell measurement is considerably below the present theoretical value of 2×1.0011596, but it has recently been re-evaluated by Hardy and Purcell[22] with the result that $g_e=2(1.001156\pm0.0000015)$.

In addition to the foregoing derived results on the g factor of the free electron, a direct measurement, by an optical pumping technique, which compares the g factor of the free electron to that of the sodium ground state has been reported by Dehmelt.[23] The result agrees with other determinations, within the rather large standard deviation, 30 parts per 10^6. A direct method, employing the induction of spin state transitions of free electrons trapped in a magnetic field has been described by Bloch,[24] but the experiment has not yielded results.

In comparing our result with the theoretical value, it is of interest to state it in terms of powers of the fine-structure constant.

Theory: $a=\alpha/2\pi-0.328\alpha^2/\pi^2$,

Present experiment: $a=\alpha/2\pi-(0.1\pm0.4)\alpha^2/\pi^2$.

ACKNOWLEDGMENTS

The authors are indebted to Dr. Donald F. Nelson, Professor G. W. Ford, and Professor R. R. Lewis for many helpful discussions; to Mr. Harry Westrick for the mechanical construction of all of the apparatus and the design of much of it; to Mr. Bruce Gehman and Mr. Paul Coleman for assistance throughout the course of the experiments.

[14] P. Kusch and H. Taub, Phys. Rev. **75**, 1477 (1949).
[15] P. Kusch and H. M. Foley, Phys. Rev. **74**, 250 (1948).
[16] S. H. Koenig, A. G. Prodell, and P. Kusch, Phys. Rev. **88**, 191 (1952).
[17] R. Beringer and M. A. Heald, Phys. Rev. **95**, 1474 (1954).
[18] J. S. Geiger, V. W. Hughes, and H. E. Radford, Phys. Rev. **105**, 183 (1957).
[19] J. W. M. DuMond, IRE Trans. on Instrumentation **I-7**, 136 (1958).
[20] J. H. Gardner and E. M. Purcell, Phys. Rev. **76**, 1262 (1949); J. H. Gardner, Phys. Rev. **83**, 996 (1951).
[21] P. Franken and S. Liebes, Jr., Phys. Rev. **104**, 1197 (1956).
[22] W. A. Hardy and E. M. Purcell (private communication).
[23] H. G. Dehmelt, Phys. Rev. **109**, 381 (1958).
[24] F. Bloch, Physica **19**, 821 (1953).

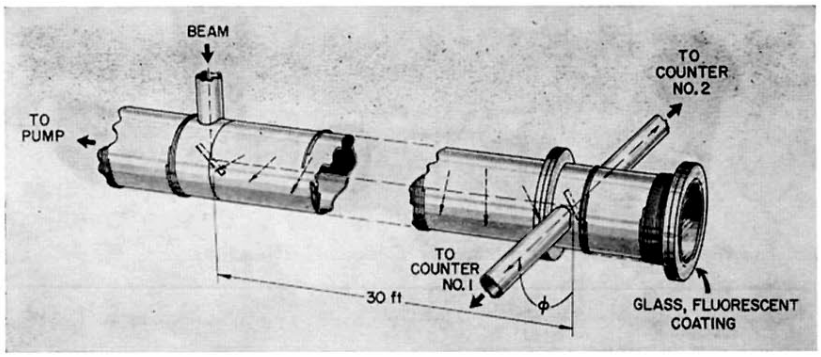

FIG. 1. Schematic diagram of the first apparatus for the measurement of the rotation of the plane of polarization of an electron beam in a magnetic field. The arrows indicate the change in the polarization along the path followed by the electrons.

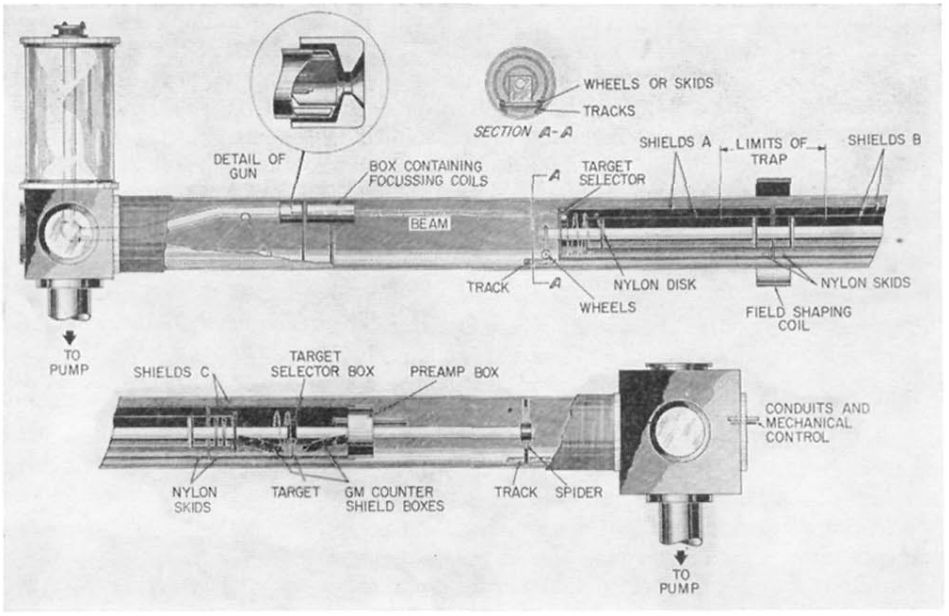

FIG. 3. Drawing of the entire vacuum chamber, including the inner parts.